IEEE Open Journal of Vehicular Technology

Received 13 June 2023; accepted 27 July 2023. Date of publication 1 August 2023;
date of current version 15 August 2023. The review of this article was coordinated by Editor Chenhao Qi.

Digital Object Identifier 10.1109/OJVT.2023.3300448

Experimental Study of Simplified UTW-OFDM Receiver Technology for Application to 5G Using Software-Defined Radio Platform

YUU ICHIKAWA, KEIICHI MIZUTANI (Member, IEEE), AND HIROSHI HARADA (Member, IEEE)

Graduate School of Informatics, Kyoto University, Kyoto 606-8501, Japan

CORRESPONDING AUTHOR: HIROSHI HARADA (e-mail: hiroshi.harada@i.kyoto-u.ac.jp).

This work was supported by the MIC/SCOPE under Grant JP196000002. An earlier version of this paper was presented in part at the 2021 IEEE 94th Vehicular Technology Conference (VTC2021-Fall), Virtual Conference, Sep.–Oct. 2021 [DOI: 10.1109/VTC2021-Fall52928.2021.9625571].

ABSTRACT The simplified universal time-domain windowed-orthogonal frequency-division multiplexing (Simplified UTW-OFDM) has been proposed to improve spectral efficiency. This study proposed a novel receiving method using an optimal inter-carrier interference (ICI) cancellation technique to improve communication quality during the application of the simplified UTW-OFDM to 5G. The simplified UTW-OFDM suppresses out-of-band emission (OOBE) through the application of very long time-domain windowing to the conventional OFDM with a cyclic prefix (CP-OFDM) symbol. However, in exchange for the OOBE suppression performance, a large ICI is generated due to the symbol distortion caused by the application of the time-domain window, resulting in the degradation of the reception quality. Therefore, in this study, we proposed a new method for calculating the log-likelihood ratio that takes into account the effect of the time-domain window. Further, an ICI canceller that included a process for suppressing the noise enhancement effect of the time-domain window was proposed. The effectiveness of the proposed method was evaluated through computer simulations and experiments using software-defined radio. The experimental evaluation showed that the proposed ICI canceller could suppress the OOBE by 23.5 dB compared to CP-OFDM under the condition that BLER of 0.1 is achieved even when 64QAM is applied.

INDEX TERMS OFDM, UTW-OFDM, 5G, local 5G, spectrum efficiency, inter-carrier interference, out-of-band emission.

I. INTRODUCTION

The 5th generation mobile communication system (5G) operated by telecommunications carriers [2] and local 5G (L5G) operated by private operators [3], [4], [5] are becoming increasingly popular. The number of users to be accommodated is expected to increase, and it is necessary to improve spectral utilization efficiency [5], [6], [7]. One solution for this issue is the suppression of out-of-band emission (OOBE) of the transmitted signal. In both 5G and L5G, cyclic-prefix orthogonal frequency division multiplexing (CP-OFDM) [8], [9] has been applied to the physical layer. However, the large OOBE caused by the discontinuity between OFDM symbols in CP-OFDM necessitates using a large guard band between frequency channels, thereby decreasing spectral efficiency [10].

Various physical layer waveforms have been proposed to suppress OOBE [11], [12], [13], [14], [15], [16], [17], [18], [19], [20], [21], [22], [23]. These can be broadly divided into filtering-based [12], [13], [14], [15], [16], [17] and time-domain windowing-based [18], [19], [20], [21], [22], [23], [24], [25], [26], [27] methods. Although the filtering-based methods can reduce OOBE effectively by convoluting the tap coefficients of the filter, they require the number of multiplications corresponding to the number of taps. If OOBE needs to be significantly suppressed (e.g., more than 50 dB) within a narrow guard band, the number of taps can be several hundred

or more, increasing the implementation complexity [17], [21]. Conversely, the time-domain windowing methods can reduce OOBE with slight implementation complexity because fewer multiplications are required for the implementation [18], [19], [20], [21], [22], [23], [24], [25], [26], [27]. Very short-time windowing has already been applied in CP-OFDM-based systems (e.g., IEEE 802.11). There has also been a lot of research on the time-domain window-based OFDM for the beyond 5G and 6G [18], [19], [20], [21], [22], [23], [24], [25], [26], [27]. In particular, universal time-domain windowed OFDM (UTW-OFDM) is a technique that can strongly suppress OOBE via the application of a long time-domain window (i.e., UTW) [20], [21], [22]. Although the long time-domain windowing shaves off part of the OFDM symbol and generates an inter-carrier interference (ICI), causing a communication quality degradation, this degradation is mitigated by strong error correction coding schemes, such as convolutional coding, turbo coding, and low-density parity check (LDPC) coding, in UTW-OFDM [20], [21], [22]. There are two types of UTW-OFDM schemes. The first is for long-delay multipath environments, wherein UTW is applied after overlapping adjacent symbols [23]. The second is a simplified UTW-OFDM scheme for short-delay multipath environments, wherein UTW is applied without overlapping adjacent symbols [1], [23]. The former was initially proposed for TV white space band wireless LAN systems (i.e., IEEE 802.11af) [20], and its applicability to LTE [21] and 5G [22] has since been studied. However, although the simplified UTW-OFDM scheme has been studied for application to LTE using turbo codes [23], there are no studies on its application to 5G using LDPC codes.

This study proposes a 5G system that uses simplified UTW-OFDM and a receiver-side signal processing technique that mitigates the receive quality degradation due to the effects of UTW applied at the transmitter side. Although the OOBE suppression performance itself is solely determined by the signal processing at the transmitter side, there is a limit to the applicable window length under the condition of achieving a certain receive quality. The purpose of this article is to propose a receiver technology that can improve the suppressible OOBE by increasing the applicable window length under conditions that can achieve a BLER of 0.1 or less, thereby suppressing the effect of ICI generated by the window applied at the transmitter side. To obtain appropriate coding gain, the 5G-compliant LDPC requires additional processing to consider the effect of the window applied at the transmitter side (e.g., ICI) in the process of log-likelihood ratio (LLR) calculation performed during decoding [22]. Therefore, this study investigates the LLR adjustment effect in the simplified UTW-OFDM applied 5G system. In addition, as the mitigation effect of ICI using only LDPC coding is limited, particularly in high-order modulation schemes such as 64QAM, we also propose and apply an ICI canceller based on the scheme proposed in [1], with additional improvements to suppress noise enhancement effects. These proposed receiving technologies for the simplified UTW-OFDM utilized 5G are evaluated through not only computer simulations but also experimental studies using software-defined radio (SDR).

In our prior and shorter version of this study [1], we proposed the basic concept of the simplified UTW-OFDM-utilized 5G system and ICI canceller. In addition, the proposed system was evaluated with QPSK and 64QAM [1] via developed link-level computer simulations. The proposed ICI canceller has adjustment coefficients with different optimal values for each UTW length. In [1], these optimal values were determined by simulation in a fully exploratory manner. In this article—the extended version of that study—, we express the signal-to-interference/noise ratio (SINR) after ICI cancellation in a mathematical expression and propose an analytical method to find the adjustment factor of the ICI canceller that can increase this SINR the most. The proposed system was evaluated with not only QPSK and 64QAM but also 16QAM. Furthermore, the proposed system was implemented based on a 5G-based SDR platform [28] to evaluate its actual performance with QPSK and 64QAM, and its effectiveness was demonstrated on actual equipment.

The main contributions of this study can be summarized as follows:

- A novel receiving technique (optimal ICI canceller to mitigate SINR degradation due to time window) when Simplified UTW-OFDM was applied to 5G.
- OOBE suppression performance and block error rate (BLER) characteristics of the proposed receiving technique were evaluated via computer simulations.
- A 5G physical layer with simplified UTW-OFDM, including the proposed receiver technology, was implemented in an SDR-based actual system, and the effectiveness of the proposed system was experimentally demonstrated.

The remainder of this article is organized as follows. Section II provides an overview of the conventional waveform shaping techniques. Section III presents the proposed simplified UTW-OFDM receiver-side processes, including optimal ICI canceller. Section IV presents an evaluation of the proposed scheme by developing 5G-based link-level computer simulations. Further, Section V demonstrates the results of SDR. Finally, Section VI offers the conclusion of this article.

II. CP-OFDM AND SIMPLIFIED UTW-OFDM

This section describes the transceiver configuration and signal processing of the conventional CP-OFDM and simplified UTW-OFDM.

A. CP-OFDM

1) TRANSMITTER

Fig. 1 shows a block diagram of the CP-OFDM transmitter. First, the transmission bit sequence is encoded by LDPC code and modulated to obtain the complex transmission symbols.

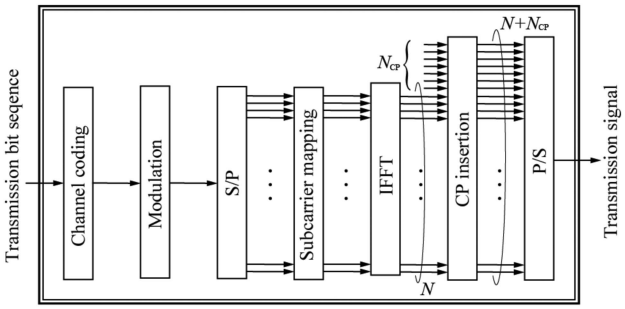

FIGURE 1. Block diagram of CP-OFDM transmitter.

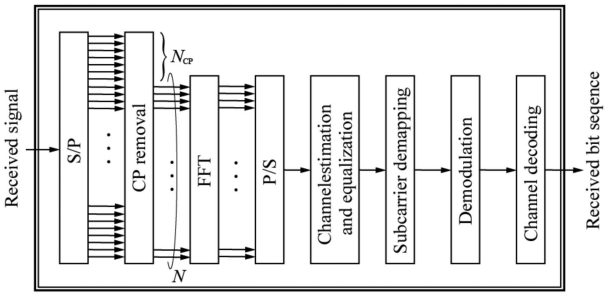

FIGURE 2. Block diagram of CP-OFDM receiver.

Next, the obtained symbols are allocated to the frequency-domain subcarriers. Thereafter, the m-th CP-OFDM symbols, $\boldsymbol{s}_m \in \mathbb{C}^{(N+N_{\mathrm{CP}})\times 1}$, are generated via the application of inverse fast Fourier transform (IFFT) to the subcarriers and by inserting CP:

$$\boldsymbol{s}_m = \boldsymbol{C}\boldsymbol{F}^{-1}\boldsymbol{x}_m, \tag{1}$$

where N is the IFFT size, N_{CP} is the number of sample points for the CP, $\boldsymbol{x}_m = [x_{(m,0)}, \ldots, x_{(m,N-1)}]^{\mathrm{T}} \in \mathbb{C}^{N\times 1}$ denotes the transmission complex symbols in the frequency domain (i.e., subcarrier symbols), $\boldsymbol{F}^{-1} \in \mathbb{C}^{N\times N}$ is the IFFT matrix, whose elements are $\boldsymbol{F}^{-1}(p,q) = \exp(\mathrm{j}2\pi pq/N)/\sqrt{N}$, where $0 \le p < N$, $0 \le q < N$, and $\boldsymbol{C} = [\boldsymbol{G}^{\mathrm{T}}, \boldsymbol{I}_N^{\mathrm{T}}]^{\mathrm{T}} \in \mathbb{Z}^{(N+N_{\mathrm{CP}})\times N}$ is the CP insertion matrix, where $\boldsymbol{G} = [0^{N_{\mathrm{CP}}\times(N-N_{\mathrm{CP}})}, \boldsymbol{I}_{N_{\mathrm{CP}}}]$. Here, $0^{i\times j}$ is an i-by-j matrix with all zero elements and $\boldsymbol{I}_N$ is an N-by-N identity matrix.

2) RECEIVER

Fig. 2 shows a typical block diagram of the CP-OFDM receiver. First, the CP is removed from the received signal, and then the frequency-domain complex symbols, $\boldsymbol{y}_m \in \mathbb{C}^{N\times 1}$ are obtained by applying fast Fourier transform (FFT):

$$\begin{aligned}\boldsymbol{y}_m &= \boldsymbol{F}\boldsymbol{D}\left(\boldsymbol{H}\boldsymbol{s}_m + \boldsymbol{n}_m\right)\\ &= \boldsymbol{F}\boldsymbol{D}\left(\boldsymbol{H}\boldsymbol{C}\boldsymbol{F}^{-1}\boldsymbol{x}_m + \boldsymbol{n}_m\right),\end{aligned} \tag{2}$$

where $\boldsymbol{n}_m \in \mathbb{C}^{(N+N_{\mathrm{CP}})\times 1}$ denotes the zero-mean complex AWGN, $\boldsymbol{H} \in \mathbb{C}^{(N+N_{\mathrm{CP}})\times(N+N_{\mathrm{CP}})}$ represents the channel matrix, $\boldsymbol{D} = [\,0^{N\times N_{\mathrm{CP}}}, \boldsymbol{I}_N]^{\mathrm{T}} \in \mathbb{Z}^{N\times(N+N_{\mathrm{CP}})}$ is the CP removal matrix, and $\boldsymbol{F} \in \mathbb{C}^{N\times N}$ denotes the FFT matrix, whose elements are $\boldsymbol{F}(p,q) = \exp(-\mathrm{j}2\pi pq/N)/\sqrt{N}$. If the multipath delay is longer than the CP length, or if carrier frequency offset (CFO) occurs, ICI will occur, and the reception quality will be degraded. However, several ICI compensation methods have been proposed for these ICIs [29], [30], [31].

Following the application of channel estimation and equalization to $\boldsymbol{y}_m$, the received bit sequence is obtained through demodulation and channel decoding.

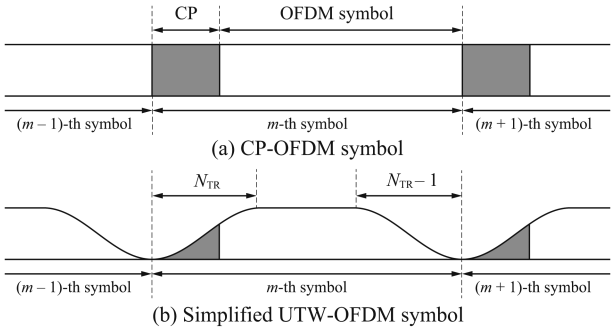

FIGURE 3. Signal waveforms of each OFDM scheme.

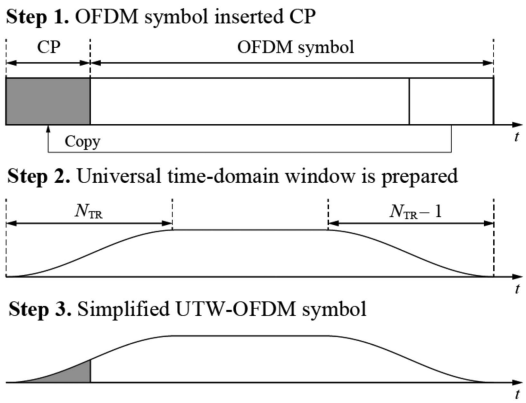

FIGURE 4. Generation procedure of simplified UTW-OFDM transmission signal.

B. SIMPLIFIED UTW-OFDM

In systems operating in multipath low-latency environments (e.g., local 5G), the maximum Doppler delay is sufficiently shorter than the CP length, resulting in a surplus of CP length. Considering this extra CP length, UTW-OFDM, wherein overlap margin (OM) processing is omitted as shown in Fig. 3(b), is referred to as simplified UTW-OFDM [1], [23]. This section describes the transmitter and receiver configurations for applying Simplified UTW-OFDM to 5G systems.

1) TRANSMITTER

Fig. 4 shows the generation procedure of the simplified UTW-OFDM transmission signals, and Fig. 5 shows a block diagram of the simplified UTW-OFDM transmitter. First, the CP-OFDM symbol, $\boldsymbol{s}_m$, is generated as shown in the previous section. Subsequently, the simplified UTW-OFDM symbol,

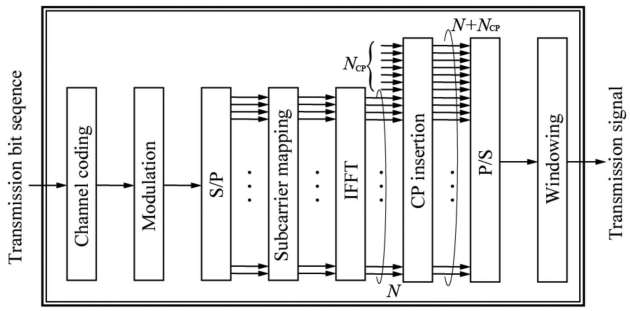

FIGURE 5. Block diagram of simplified UTW-OFDM transmitter.

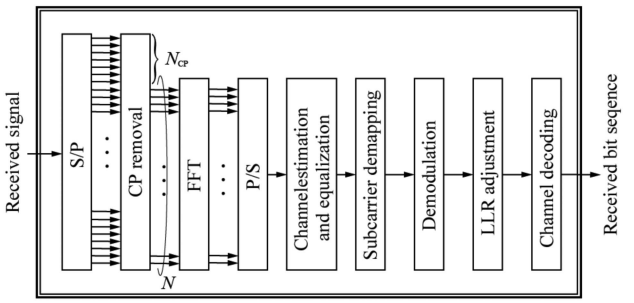

FIGURE 6. Block diagram of simplified UTW-OFDM receiver.

$\boldsymbol{s}_m^{\mathrm{UTW}}$, is obtained by applying the time-domain window as follows:

$$\begin{aligned}\boldsymbol{s}_m^{\mathrm{UTW}} &= \boldsymbol{W}\boldsymbol{s}_m \\ &= \boldsymbol{W}\boldsymbol{C}\boldsymbol{F}^{-1}\boldsymbol{x}_m,\end{aligned} \tag{3}$$

where $\boldsymbol{W} \in \mathbb{C}^{(N+N_{\mathrm{CP}})\times(N+N_{\mathrm{CP}})}$ is time-domain windowing matrix defined as follows:

$$\boldsymbol{W} = \mathrm{diag}\,(\boldsymbol{w}), \tag{4}$$

$$\boldsymbol{w} = \begin{bmatrix} \boldsymbol{w}_{\mathrm{TR}} \\ 1^{(N+N_{\mathrm{CP}}-2N_{\mathrm{TR}}+1\ )\times 1} \\ \boldsymbol{w}_{\mathrm{TR}}^{\mathrm{I}} \end{bmatrix}, \tag{5}$$

where diag(·) denotes the diagonal matrix with the components in the parentheses as diagonal components, $\boldsymbol{w} \in \mathbb{C}^{(N+N_{\mathrm{CP}})\times 1}$ represents the simplified UTW vector, and $\boldsymbol{w}_{\mathrm{TR}} \in \mathbb{C}^{N_{\mathrm{TR}}\times 1}$ and $\boldsymbol{w}_{\mathrm{TR}}^{\mathrm{I}} \in \mathbb{C}^{(N_{\mathrm{TR}}-1)\times 1}$ are the UTW and inverse UTW transition vectors, respectively, N_{TR} represents transition length of the time-domain window, where $0 \le N_{\mathrm{TR}} \le N/2$. Further, here, $\mathbf{1}^{i\times j}$ is an i-by-j matrix with all elements set to one. When $N_{\mathrm{TR}} = 0$, the transmitted signal is identical to that of a CP-OFDM. This study uses a raised cosine window defined by the following equation as the time-domain window:

$$w_m = \sin^2\left(\frac{\pi m}{N_{\mathrm{TR}}}\right), \tag{6}$$

where w_m is the m-th component of $\boldsymbol{w}_{\mathrm{TR}}$.

2) RECEIVER

a) Overview of the receiver configuration: The block diagram of the conventional simplified UTW-OFDM receiver is shown in Fig. 6. The m-th received symbol sequence, $\boldsymbol{y}_m^{\mathrm{UTW}}$, is expressed as follows:

$$\begin{aligned}\boldsymbol{y}_m^{\mathrm{UTW}} &= \boldsymbol{F}\boldsymbol{D}\left(\boldsymbol{H}\boldsymbol{s}_m^{\mathrm{UTW}} + \boldsymbol{n}_m\right) \\ &= \boldsymbol{F}\boldsymbol{D}\left(\boldsymbol{H}\boldsymbol{W}\boldsymbol{C}\boldsymbol{F}^{-1}\boldsymbol{x}_m + \boldsymbol{n}_m\right),\end{aligned} \tag{7}$$

After demodulating $\boldsymbol{y}_m^{\mathrm{UTW}}$ with channel estimation and equalization, the received bit sequence can be obtained through LLR adjustment [18] and channel decoding.

b) LLR adjustment technique: The absolute value of the LLR (i.e., the certainty of the code) used for LDPC decoding is inversely proportional to the noise power [22]. Therefore, the absolute value of LLR is considerably large in high SNR environments. However, in the case of simplified UTW-OFDM, ICI is caused by the loss of OFDM orthogonality owing to the application of the time-domain window with a transition length that exceeds the CP length at the transmitter side. Consequently, this ICI results in the absolute value of LLR to be calculated being calculated mainly for the wrong direction. The solution to this problem is LLR adjustment, which normalizes the absolute value of LLR. When the average value of LLR is normalized to m, the adjusted LLR, λ_j', is expressed as follows:

$$\lambda_j' = \frac{m}{\frac{1}{n}\sum_{k=1}^{n}\lambda_k}\lambda_j, \tag{8}$$

where λ_j is the j-th original LLR. In this article, m is assumed to be 4 [22].

III. PROPOSED SIMPLIFIED UTW-OFDM RECEIVING TECHNIQUE WITH OPTIMAL ICI CANCELLER

In this section, we propose an optimal ICI canceller with noise enhancement suppression to improve the reception quality of 5G systems using simplified UTW-OFDM. Since simplified UTW-OFDM is designed to operate in a short multipath delay environment, ICI due to delayed waves exceeding the CP length does not occur. Furthermore, because frequency synchronization between the base station and user equipment is precisely implemented by using the global navigation satellite system (GNSS) in 5G, it is safe to assume that ICI due to CFO is not generated. However, even in such a situation, ICI is generated by setting a UTW length that exceeds the CP length. The purpose of the proposed method is to suppress the effect of ICI caused by UTW.

A. PROPOSED ICI CANCELLER WITH NOISE ENHANCEMENT SUPPRESSION

The proposed method suppresses the ICI caused by the UTW multiplied at the transmitter side through the multiplication of the ICI cancellation matrix in the frequency domain at the receiver side. The ICI cancellation matrix is generated via the multiplication of the inverse function of the known UTW, obtained based on the minimum mean square error (MMSE)

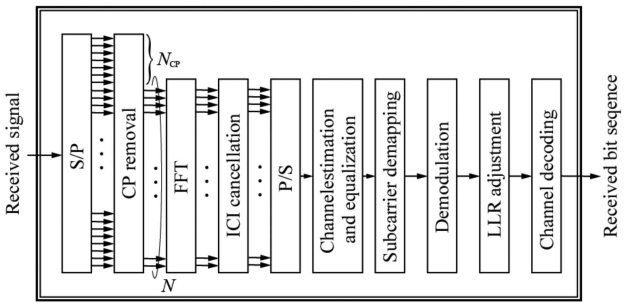

FIGURE 7. Block diagram of simplified UTW-OFDM receiver with ICI canceller.

method, through an adjustment weight to reduce the noise enhancement effect.

Fig. 7 shows a block diagram of the simplified UTW-OFDM receiver applying the proposed ICI canceller. As the demodulation reference signal (DM-RS), which is the reference signal when performing channel estimation, is also affected by ICI due to the application of UTW, the proposed ICI canceller is applied prior to performing channel estimation and equalization. The m-th received symbol, $\boldsymbol{y}_m^{\mathrm{IC}} \in \mathbb{C}^{N\times 1}$, with the proposed ICI canceller is expressed as follows:

$$\begin{aligned}\boldsymbol{y}_m^{\mathrm{IC}} &= \boldsymbol{PFD}\left(\boldsymbol{H}\boldsymbol{s}_m^{\mathrm{UTW}} + \boldsymbol{n}_m\right)\\ &= \boldsymbol{PFD}\left(h_0\boldsymbol{I}_{N+N_{\mathrm{CP}}} + \boldsymbol{H}^{\mathrm{D}}\right)\boldsymbol{WCF}^{-1}\boldsymbol{x}_m + \boldsymbol{n}_m^{\mathrm{IC}}\\ &= h_0\boldsymbol{PFDWCF}^{-1}\boldsymbol{x}_m + \boldsymbol{PFDH}^{\mathrm{D}}\boldsymbol{WCF}^{-1}\boldsymbol{x}_m + \boldsymbol{n}_m^{\mathrm{IC}}, \quad (9)\end{aligned}$$

$$\boldsymbol{n}_m^{\mathrm{IC}} = \boldsymbol{PFDn}_m, \quad (10)$$

where $\boldsymbol{P} \in \mathbb{C}^{N\times N}$ is the ICI cancellation matrix, h_0 is the time-domain channel gain of the first arrival wave, $\boldsymbol{H}^{\mathrm{D}} \in \mathbb{C}^{(N+N_{\mathrm{CP}})\times(N+N_{\mathrm{CP}})}$ is the channel matrix with the delayed wave components (i.e., $h_0\boldsymbol{I}_{N+N_{\mathrm{CP}}} + \boldsymbol{H}^{\mathrm{D}} = \boldsymbol{H}$), and $\boldsymbol{n}_m^{\mathrm{IC}}$ is the effective noise when the ICI canceller is applied to the UTW-OFDM-applied 5G system. Originally, the purpose of multiplying $\boldsymbol{P}$ is to cancel the ICI generated by $\boldsymbol{HW}$ when applying a time window with a transition length that exceeds the CP length. Here, as mentioned in Section II-B, the simplified UTW-OFDM is originally designed for multipath environments with low delay. Therefore, the receiver design in this study suppresses the ICI generated by the combination of UTW and the main path (first arrival wave), which is expected to have a dominant effect on the reception quality. In other words, the $\boldsymbol{P}$ is designed to reduce the ICI effect generated by UTW in the component of $h_0\boldsymbol{PFDWCF}^{-1}\boldsymbol{x}_m$ in (9). Then the ICI cancellation matrix, $\boldsymbol{P}$, is calculated by using MMSE as follows:

$$\boldsymbol{P} = \left(\boldsymbol{A}^{\mathrm{H}}\boldsymbol{A} + \frac{N_0}{E_{\mathrm{s}}}\boldsymbol{I}_N\right)^{-1}\boldsymbol{A}^{\mathrm{H}}, \quad (11)$$

$$\boldsymbol{A} = \boldsymbol{FD}\left\{(1-\alpha)\boldsymbol{I}_{N+N_{\mathrm{CP}}} + \alpha\boldsymbol{W}\right\}\boldsymbol{CF}^{-1}, \quad (12)$$

where $(\cdot)^{\mathrm{H}}$ denotes the complex conjugate transpose of the matrix in the bracket, N_0 is the noise power spectral density, E_{s} is the energy per one symbol transmission, α is the adjustment factor to mitigate noise enhancement at the OFDM symbol edge (NEOSE), and $\boldsymbol{A}^{-1}$ is the zero-forcing weight to obtain $\boldsymbol{x}_m$ (when $\alpha = 1$, $\boldsymbol{A} = \boldsymbol{FDWCF}^{-1}$). Although it is difficult to remove the ICI component due to the combination of UTW and delayed wave components with the designed $\boldsymbol{P}$, the ICI effect suppression can be performed without using the channel estimation results. Therefore, channel estimation using DM-RS can be performed after suppressing the ICI effect. In addition, as mentioned above, since an environment with small delayed waves is assumed, the residual ICI that cannot be suppressed is expected to be small.

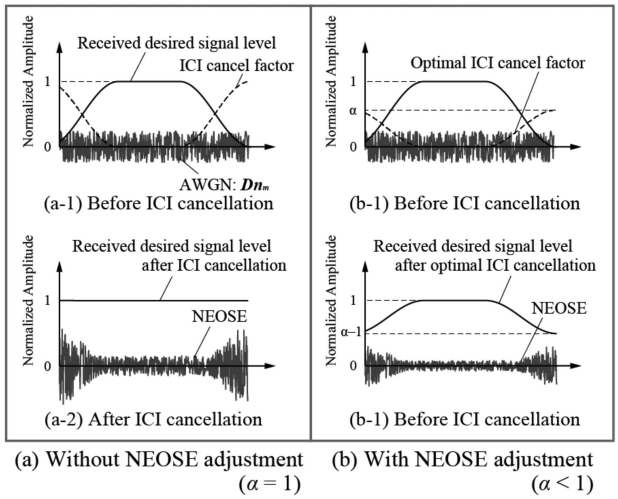

FIGURE 8. Noise enhancement at OFDM symbol edge.

First, let us consider the case where α is 1 (i.e., no adjustment). Before ICI cancellation. In this case, the amplitude of the OFDM symbol edge is depressed by UTW multiplication at the transmitter side, as shown in Fig. 8(a-1). These symbol edge depressions are amplified via the multiplication of the ICI cancellation matrix at the receiver side, and a flat amplitude characteristic is attempted, as shown in Fig. 8(a-2). However, as shown in (9) and (10), the ICI cancellation matrix is applicable to both the desired signal and the noise components. Therefore, the noise in (10) is over-amplified at the symbol edge (i.e., NEOSE is generated) by $\boldsymbol{W}$ used in (12), as shown in Fig. 10(a-2). Consequently, the communication quality is degraded.

However, α is appropriately adjusted (Fig. 8(b-1)), this NEOSE generation can be suppressed. The smaller the value of α, the greater NEOSE suppression; however, the ICI cancellation performance degrades (Fig. 8(b-2)). Therefore, there exists a trade-off between the reduction of NEOSE and ICI cancellation performance, and it is necessary to adjust α considering these trade-offs.

B. DESIGN OF OPTIMAL NEOSE ADJUSTMENT FACTOR α

Owing to a trade-off relationship between NEOSE generation and ICI cancellation performance, an appropriate α must be designed. Therefore, the relationship between α and SINR after ICI cancellation is formulated. Using the formulation to be

developed, the α that achieves the highest SINR is determined as the optimal α.

In the formulation, to calculate SINR, the desired signal components are identical matrices with each modulation subcarrier symbol as one. In addition, additive white Gaussian noise (AWGN) is used as the noise component. The propagation path is assumed to be ideal (i.e., $\boldsymbol{H} = \boldsymbol{I}_{N+N_{\mathrm{CP}}}$) because the purpose is to express in SINR only the effect of residual ICI and enhanced noise when signal processing is performed to cancel ICI generated by the application of a time window with a transition length that exceeds the CP length. The matrix with desired and interference signal components for each subcarrier, $\boldsymbol{Y}^{\alpha} \in \mathbb{C}^{N\times N}$, is expressed as follows:

$$\boldsymbol{Y}^{\alpha} = \boldsymbol{PFD}\left(\boldsymbol{WCF}^{-1}\boldsymbol{I}_N + \mathrm{diag}\left(\boldsymbol{n}_m\right)\right), \tag{13}$$

where the diagonal component of $\boldsymbol{Y}^{\alpha}$ ($y^{\alpha}_{k,\,k}$, $0 \le k < N$) denotes the desired signal component, and remaining component ($y^{\alpha}_{i,\,k}$, $0 \le i < N$, $i \ne k$) denotes the interference component. Therefore, the SINR, $\beta(\alpha)$, which is defined as a function of α, is expressed as follows:

$$\beta\left(\alpha\right) = \frac{1}{N}\sum_{k=1}^{N}\frac{\left(y^{\alpha}_{k,\,k}\right)^2}{\sum_{i\ne k}\left(y^{\alpha}_{i,\,k}\right)^2}. \tag{14}$$

Therefore, if the number of subcarriers to be used is known, the optimal α can be calculated in advance using (14) as follows;

$$\alpha_{\mathrm{opt}} = \arg\max\left(\beta\left(\alpha\right)\right). \tag{15}$$

Note that these calculations are not performed during communication, but rather the α_{opt} for the UTW length is calculated in advance.

C. COMPUTATIONAL COMPLEXITY OF PROPOSED ICI CANCELLER

The ICI canceller proposed in this article is a technique to cancel ICI (i.e., ICI artificially generated to suppress OOBE) caused by a time window with a transition length longer than the CP length applied at the transmitter side. As can be seen from (11) and (12), the ICI cancellation matrix $\boldsymbol{P}$ is uniquely determined once the type of time window, the transition length, and α are determined and can be calculated in advance. Also, as shown in (9), ICI cancellation is completed simply by multiplying the subcarrier signal (the signal sequence after FFT) obtained by ordinary CP-OFDM by the pre-computed $\boldsymbol{P}$. The size of this calculation is about the same as that of the FFT, which is a perfectly acceptable increase in computational complexity given the capabilities of recent signal-processing hardware.

IV. EVALUATION BY COMPUTER SIMULATIONS

In this section, we evaluate the proposed receiving method applied to simplified UTW-OFDM using 5G-based link-level computer simulations. First, the optimal α is calculated employing the proposed numerical model (i.e., (14) and (15)) and compared with the optimal α obtained by the link-level simulation to validate the proposed model and to determine the α to be used in the evaluation. Subsequently, the OOBE suppression performance and BLER characteristics are evaluated assuming L5G applications. The simulation parameters [32], [33], [34], [35], [36] are listed in Table 1. Here, the modulation scheme and coding rate are set according to the modulation and coding scheme (MCS) defined by the third-generation partnership project (3GPP), and the required BLER is set to 10^{-1} [36]. The channel model applied is the extended pedestrian-A (EPA) specified by the 3GPP.

TABLE 1. Simulation Parameters for Computer Simulations

Parameter	Values
Carrier frequency	4.7 GHz
Subcarrier spacing	15 kHz
Channel bandwidth	5 MHz
Channel coding	LDPC
Decoding algorithm, iteration	Log sum-product, 50
FFT size, N	512
CP length, N_{CP}	36
MCS index,	MCS7 (QPSK),
Modulation scheme	MCS13 (16QAM),
	MCS18 (64QAM).
Channel model	3GPP-EPA
Antenna configuration	TX: 1, RX: 4 (MRC)

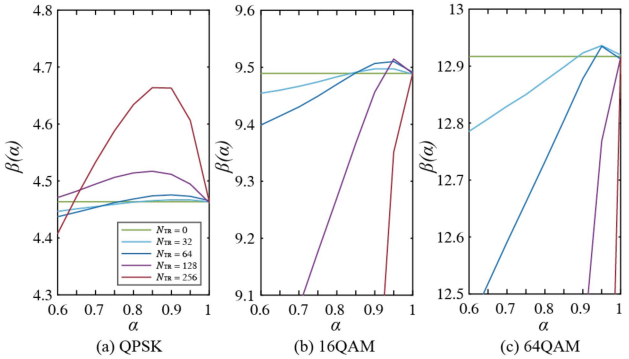

FIGURE 9. SINR as a function of α obtained by (14) and (15).

A. CALCULATING THE OPTIMAL α

The relationship between α and $\beta(\alpha)$ in QPSK, 16QAM, and 64QAM calculated based on (14) is shown in Fig. 9. The calculation was performed under the condition of E_s/N_0 to achieve BLER $= 10^{-1}$ when the ICI canceller with $\alpha = 1$ was applied to CP-OFDM. In the case of QPSK, for small N_{TR}, the variation in SINR with respect to the variation of α is small. This is because the effect of ICI owing to time-domain window multiplication is small and the improvement in communication quality by LDPC codes is large. However, when N_{TR} is large, the effect of NEOSE generated by the ICI canceller is large. Consequently, the variation in SINR with respect to α is also large. For QAM, the optimal α was close to 1. This is because the E_s/N_0 for the calculation was large (i.e., the original noise power is small), and the NEOSE generated by the application of the ICI canceller was also small.

TABLE 2. Optimal α Obtained From (14) and (15)

Modulation scheme	N_{TR}	Optimal α by (14) and (15)	Optimal α by Computer simulation
MCS7, QPSK	32	0.9	0.9
	64	0.9	0.9
	128	0.85	0.85
	256	0.85	0.85
MCS13, 16QAM	32	0.9	0.9
	64	0.95	0.9
	128	0.95	0.95
	256	1	1
MCS18, 64QAM	32	0.95	0.95
	64	0.95	0.95
	128	1	1
	256	1	1

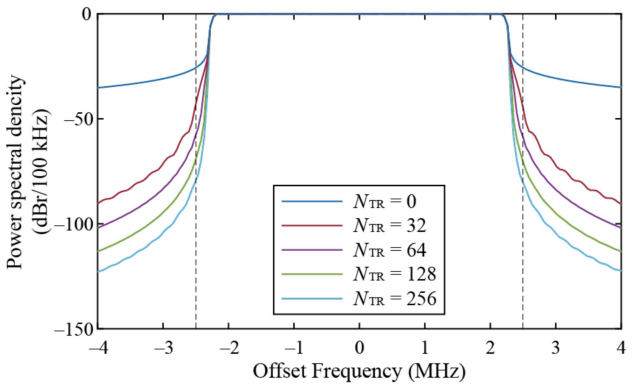

FIGURE 10. OOBE suppression performance.

The optimal α obtained using (14) and (15) and that obtained by computer simulation (α with the minimum BLER) are presented in Table 2. The optimal values obtained were equivalent to those obtained through the computer simulations, thus validating (14) and (15). In this study, the ICI canceller applicable for the optimal α for each MCS and N_{TR} is referred to as the optimal ICI canceller.

B. OOBE SUPPRESSION PERFORMANCE

Fig. 10 shows the transmitted signal spectrum of the simplified UTW-OFDM-applied 5G system. The vertical axis represents the averaged power spectral density (PSD) normalized by the maximum value, and the horizontal axis represents the offset frequency from the center frequency. Further, the resolution bandwidth and oversampling factor were set to 100 kHz and 4, respectively. Moreover, $N_{TR} = 0$ is equivalent to CP-OFDM. Comparisons of the PSD at the channel edge (i.e., offset frequency of ± 2.5 MHz) confirmed that the larger N_{TR} yielded the higher OOBE suppression performance. When N_{TR} was set to 256, the OOBE at the channel edge was suppressed by 54.8 dB compared to CP-OFDM. This result is independent of the MCS.

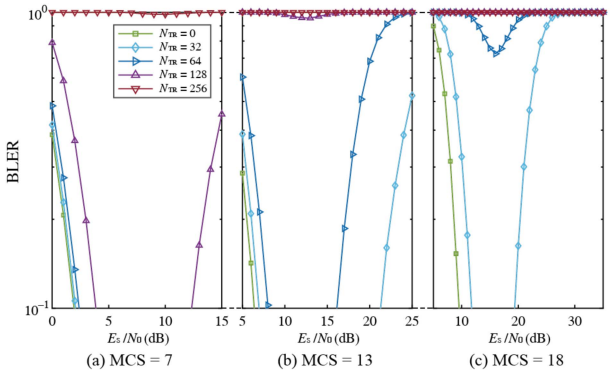

FIGURE 11. BLER characteristics without LLR adjustment and ICI canceller (conventional CP-OFDM receiver).

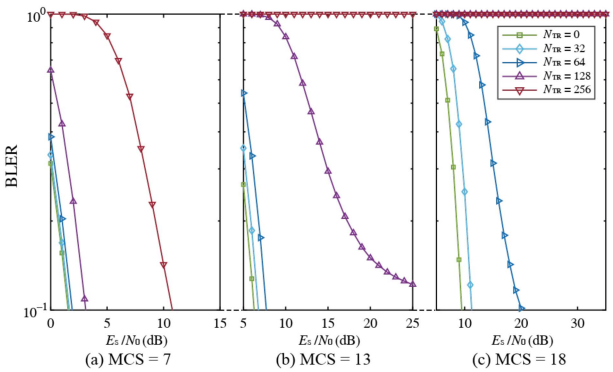

FIGURE 12. BLER characteristics with LLR adjustment and without ICI canceller.

C. BLER CHARACTERISTIC

1) BLER CHARACTERISTICS WITHOUT LLR ADJUSTMENT AND ICI CANCELLER

Fig. 11 shows the BLER characteristics of the simplified UTW-OFDM using QPSK, 16QAM, and 64QAM without using the LLR adjustment technique and ICI canceller (i.e., conventional CP-OFDM receiver). For QPSK, BLER $= 10^{-1}$ was achieved when $0 \leq N_{TR} \leq 128$. However, BLER characteristics degraded at the high E_s/N_0 environment in the case of $N_{TR} = 128$, and BLER again increased to a value greater than 10^{-1}. The BLER degradation is attributed to the very large LLRs in the wrong direction caused by ICI generated by the UTW. The impact of this problem is particularly large at high MCSs. In the case of 16QAM, BLER $= 10^{-1}$ was achieved with $N_{TR} \leq 64$. In the case of 64QAM, only $N_{TR} = 32$ achieved BLER $= 10^{-1}$. However, even in these cases of QAM, the BLER was degraded for high E_s/N_0.

2) BLER CHARACTERISTICS WITH LLR ADJUSTMENT AND WITHOUT ICI CANCELLER

Fig. 12 shows the BLER characteristics of the simplified UTW-OFDM using QPSK, 16QAM, and 64QAM with LLR adjustment technique and no ICI canceller. Through the use of LLR adjustment, the BLER degradations in high E_s/N_0 environments were improved. Consequently, BLER $= 10^{-1}$

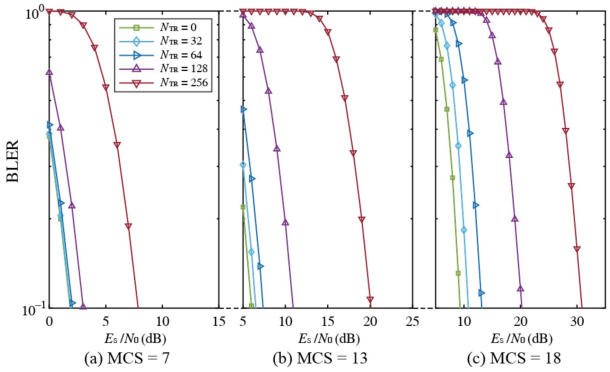

FIGURE 13. BLER characteristics with LLR adjustment and proposed optimal ICI canceller.

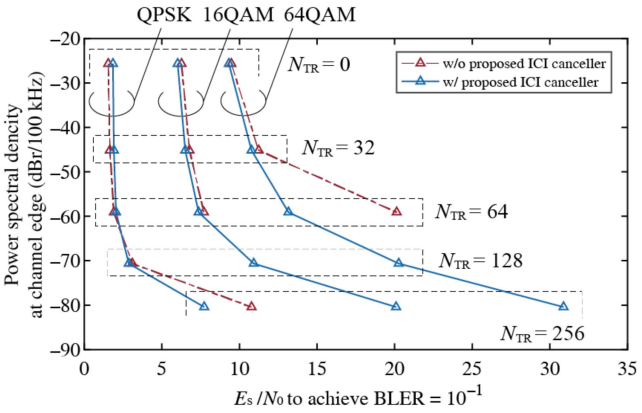

FIGURE 14. Relationship between normalized PSD at the channel edge and E_s/N_0 to achieve BLER = 10^{-1}.

was achieved when $N_{TR} \leq 256$ for QPSK and when $N_{TR} \leq 64$ for 16QAM and 64QAM. In addition, the BLER degradation problems were improved.

These results indicate that upon the application of the simplified UTW-OFDM to 5G, the degradation of the communication quality can be reduced using the LLR adjustment technique in the LDPC decoding [22]. However, when achieving OOBE suppression of 54.8 dB for QPSK and 45.0 dB for 16QAM and 64QAM, respectively, certain degradation of E_s/N_0 to achieve BLER = 10^{-1} was still observed owing to ICI generated by the time-domain window multiplying. As the impact of the ICI is still not small, the ICI should be reduced at the receiver by the ICI canceller.

3) BLER CHARACTERISTICS WITH LLR ADJUSTMENT AND PROPOSED OPTIMAL ICI CANCELLER

Fig. 13 shows the BLER characteristics of the simplified UTW-OFDM using QPSK, 16QAM, and 64QAM with the LLR adjustment and proposed optimal ICI canceller. For QPSK, the E_s/N_0 value required to achieve BLER = 10^{-1} at $N_{TR} = 256$ was improved by 2.9 dB through the application of the optimal ICI canceller, as shown in Figs. 12(a) and 13(a). Whereas, for 16QAM, the E_s/N_0 value required to achieve BLER = 10^{-1} at $N_{TR} = 64$ was improved by 0.3 dB, as shown in Figs. 12(b) and 13(b). Moreover, the BLER characteristics were also significantly improved, as BLER = 10^{-1} was achieved when $N_{TR} \geq 128$. In the case of 64QAM, the E_s/N_0 value required to achieve BLER = 10^{-1} at $N_{TR} = 64$ was improved by 7.0 dB through the application of the optimal ICI canceller, as shown in Figs. 12(c) and 13(c). Furthermore, the BLER characteristics were significantly improved, achieving BLER = 10^{-1} when $N_{TR} \geq 128$.

D. OOBE SUPPRESSION PERFORMANCE VS E_S/N_0 TO ACHIEVE REQUIRED BLER

Fig. 14 shows the relationship between the normalized PSD at the channel edge and the E_s/N_0 value required to achieve BLER = 10^{-1}. The solid and dashed lines indicate the results with the proposed optimal ICI canceller (i.e., the relationship between Figs. 10 and 13) and without the proposed optimal ICI canceller (i.e., the relationship between Figs. 10 and 12), respectively.

In the case of QPSK, the PSD at the channel edge was suppressed by 33.4 dB with nearly identical communication quality as that of CP-OFDM, regardless of the usage of the optimal ICI canceller when $N_{TR} \leq 64$. However, when $N_{TR} = 128$ and 256, upon accepting 1.0 and 5.9 dB degradation of the E_s/N_0 to achieve BLER = 10^{-1}, respectively, the simplified UTW-OFDM with the optimal ICI canceller improved the communication quality by 0.3 and 3.0 dB, respectively. Simultaneously, the PSD at the channel edge was suppressed by 45.0 and 54.8 dB, respectively, compared to that of CP-OFDM.

In the case of 16QAM, when $N_{TR} = 32$ and 64, upon accepting 0.3 and 1.4 dB degradation of the E_s/N_0 to achieve BLER = 10^{-1}, respectively, the simplified UTW-OFDM with the optimal ICI canceller improved the communication quality by 0.2 and 0.4 dB, respectively. Simultaneously, the PSD at the channel edge was suppressed by 19.5 dB and 33.4 dB, respectively, compared to that of CP-OFDM. Moreover, when $N_{TR} = 128$ and 256, BLER = 10^{-1} was achieved via the application of the optimal ICI canceller. The simplified UTW-OFDM suppressed the PSD at the channel edge by 45.0 and 54.8 dB, respectively, compared to that of CP-OFDM; in this case, the E_s/N_0 degradation values were 4.9 and 14.1 dB, respectively.

In the case of 64QAM, when $N_{TR} = 32$ and 64, upon accepting 1.5 and 3.8 dB degradation of the E_s/N_0 to achieve BLER = 10^{-1}, respectively, the simplified UTW-OFDM with the optimal ICI canceller improved the communication quality by 0.5 and 0.7 dB, respectively. Further, the PSD at the channel edge was suppressed by 19.5 and 33.4 dB, respectively, compared to that of CP-OFDM. Moreover, when $N_{TR} = 128$ and 256, BLER = 10^{-1} was achieved by applying the optimal ICI canceller, with the simplified UTW-OFDM suppressing the PSD at the channel edge by 45.0 dB and 54.8 dB, respectively, compared to that of CP-OFDM; the E_s/N_0 degradation values were 10.9 and 21.6 dB, respectively.

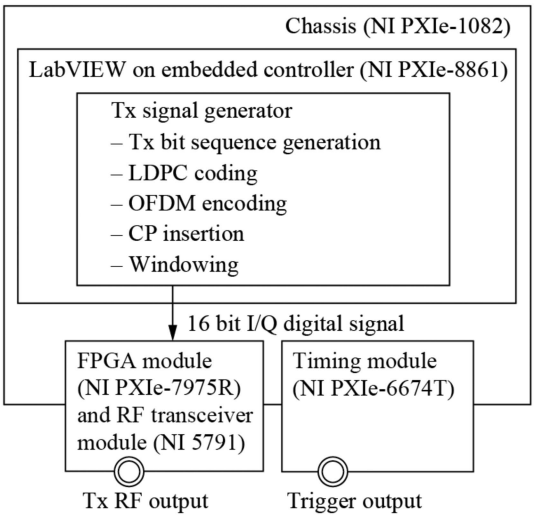

FIGURE 15. Transmitter configuration of SDR.

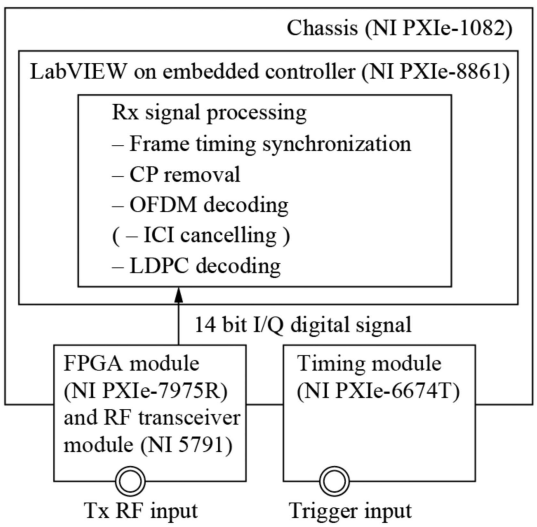

FIGURE 16. Receiver configuration of SDR.

V. EXPERIMENTAL EVALUATION BY USING SOFTWARE-DEFINED RADIO PLATFORM

In this section, the simplified UTW-OFDM and the proposed receiving technique, whose effectiveness in 5G was demonstrated via computer simulations in the previous section, are implemented using an SDR-based evaluation platform [28]. Consequently, their basic characteristics are experimentally evaluated. First, the configuration of the transmitter and receiver in the constructed experimental evaluation system and the configuration of the entire system are described. Thereafter. the simplified UTW-OFDM and the proposed receiving technique were experimentally evaluated using the constructed evaluation system, focusing on the OOBE suppression performance and BLER characteristics.

A. TRANSMITTER

Fig. 15 shows the SDR-based transmitter configuration. The transmitter comprised a chassis with a high-speed communication bus (NI PXIe-1082), an RF module (NI 5791), an FPGA module (NI PXIe-7975R), a timing module (NI PXIe-6674T), and an embedded controller (PXIe-8861). The synchronization module generated a high-precision clock, and all modules shared the same operating clock. First, 5G-based baseband signals modulated by the simplified UTW-OFDM were generated using a signal processing software (NI LabVIEW) in the embedded controller, and 16-bit I/Q digital signals were written to the FPGA module. Subsequently, the signal was converted to an analog signal using the analog-to-digital converter (ADC) and up-converted to an RF signal in the RF module.

B. RECEIVER

Fig. 16 shows the SDR-based receiver configuration. The basic configuration was identical to that of the transmitter. First, the received RF analog signal was down-converted to baseband signal in the transceiver module. Subsequently, the baseband signal was sampled via a digital-to-analog converter (DAC) to a 14-bit I/Q digital signal in the FPGA module. The sampled digital I/Q signal was then passed to the embedded controller. Thereafter, the demodulation process of the received baseband signal was performed in the signal processing software (NI LabVIEW). Further, receiver diversity in the demodulation process was achieved through the combination of the received signals obtained at different times to perform pseudo-maximum ratio combining (MRC).

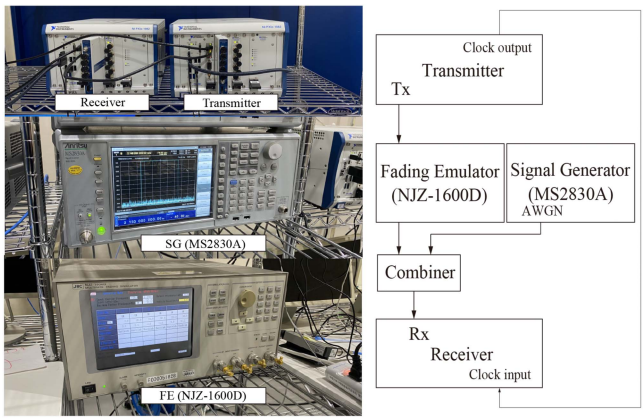

FIGURE 17. Developed experimental evaluation platform and its system configuration.

C. CONNECTION CONFIGURATION

Fig. 17 shows the developed experimental evaluation platform and its system configuration. The transmitted downlink (DL) signal was input to the fading emulator (FE, NJZ-1600D, JRC). The FE output and AWGN signals generated by the signal generator (SG, MS2830A, Anritsu) were input to a combiner (PD510-OS, R&K). Consequently, the combined signal is input to the SDR-based receiver. The operating clock

TABLE 3. Experimental Parameters for SDR

Parameter	Values
Carrier frequency	2.15 GHz
Channel bandwidth	5 MHz
Output power	–25 dBm
Reference level	–20 dBm
Sampling rate	7.672 MHz
Channel model	Modified-EPA
Moving speed	6.6 km/h
Antenna configuration	TX: 1, RX: 1

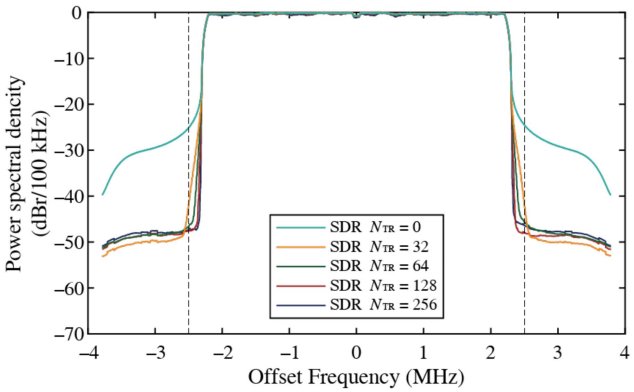

FIGURE 18. OOBE suppression performance in the experimental evaluation.

was shared by the transmitter and receiver by connecting a synchronization module via an RF cable. Therefore, the experiment was conducted assuming that the frequency offsets did not influence the outcome. The FE used in this experiment supported frequency bands up to 3 GHz and bandwidth up to 20 MHz. In addition, the upper limit of the number of paths that could be output in one channel was 6 waves.

D. EVALUATION

The parameters of the baseband signal in this evaluation were the same as those presented in Table 1, whereas the parameters specific to the SDR-based evaluation platform are presented in Table 3. Because the FE specification limits the operating frequency, the center frequency was set to 2.15 GHz, and the moving speed was applied such that the fading was equivalent to the frequency in the evaluation in Section IV (i.e., 4.7 GHz). This is valid because when modulating and demodulating baseband signals in a multipath fading environment, the only effect of differences in the frequency band is the relationship between moving speed and Doppler frequency. Consequently, as the FE could only be set up to 6 paths, the EPA model with the 7th path removed was used as the channel model.

1) OOBE SUPPRESSION PERFORMANCE

Fig. 18 shows the transmitted signal spectrum of the simplified UTW-OFDM-applied 5G system obtained through experimental evaluation. Through comparisons of the PSD at the channel edge it was confirmed that larger N_{TR} yielded

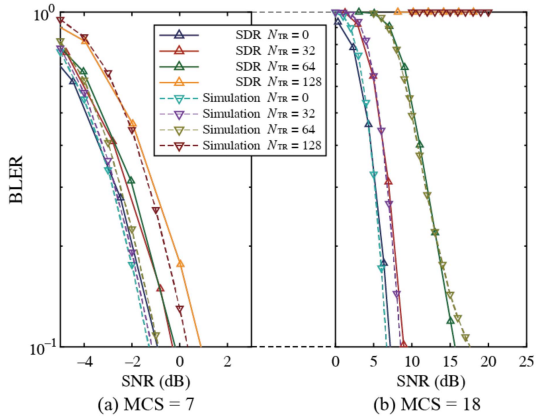

FIGURE 19. Experimentally evaluated BLER characteristics with LLR adjustment and without ICI canceller.

a higher OOBE suppression performance when $N_{TR} \leq 128$. When N_{TR} was set to 128, the OOBE at the channel edge was suppressed by 23.5 dB compared to CP-OFDM. Further, compared to the results of the computer simulation (Fig. 10), the noise floor was increased and observed at approximately –50 dB in the case of the experiment. This is because of the quantization noise from the transmitter's DAC and the receiver's ADC. Moreover, the PSD at the channel edge was degraded at $N_{TR} = 256$ compared to $N_{TR} = 128$, where the waveform shape exerted a larger effect.

2) BLER CHARACTERISTICS WITH LLR ADJUSTMENT AND WITHOUT PROPOSED ICI CANCELLER

The BLER characteristics of QPSK and 64QAM with LLR adjustment and no proposed ICI canceller are shown in Fig. 19(a) and (b), respectively. In Fig. 19, the solid and dashed lines represent the BLER obtained by the SDR-based experiment and computer simulation, respectively. The experimental results show that BLER $= 10^{-1}$ was achieved for all N_{TR} conditions where BLER $= 10^{-1}$ was achieved in the computer simulation. Thus, the essential characteristics of the 5G system with simplified UTW-OFDM were successfully verified on the actual RF device. However, compared to the computer simulation results, the SNR to achieve BLER $= 10^{-1}$ is degraded by 0.8 dB at worst, and the slope of the curve was slightly different for $N_{TR} = 64$ in the case of 64QAM. This can be attributed to the difference owing to the aforementioned FE setting limits.

3) BLER CHARACTERISTICS WITH PROPOSED ICI CANCELLER

The BLER characteristics of QPSK and 64QAM with the LLR adjustment and the proposed optimal ICI canceller are shown in Fig. 20(a) and (b), respectively. The effectiveness of the proposed optimal ICI canceller can also be confirmed in the experimental evaluation. In the case of QPSK, a comparison of Figs. 19(a) and 20(a) shows that the application of the optimal ICI canceller improved the SNR to achieve BLER $= 10^{-1}$ for all N_{TR}. For example, it was improved by 0.2 dB

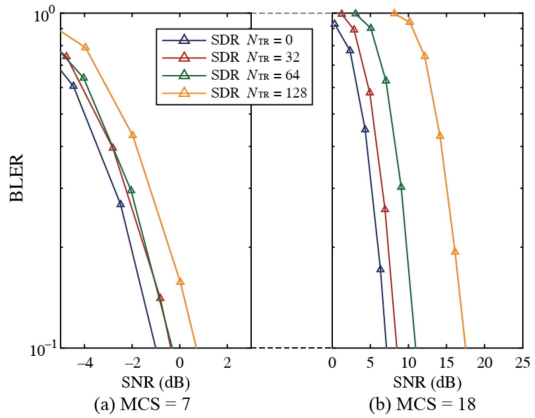

FIGURE 20. Experimentally evaluated BLER characteristics with LLR adjustment and proposed optimal ICI canceller.

at $N_{TR} = 128$. In the case of 64QAM, Figs. 19(b) and 20(b) show that the SNR to achieve BLER $= 10^{-1}$ was improved by 4.7 dB at $N_{TR} = 64$ owing to the application of the optimal ICI canceller. Moreover, the BLER characteristics were significantly improved at $N_{TR} \geq 128$, achieving BLER $= 10^{-1}$. These results indicate that the proposed method is effective for the actual experiment with the SDR.

VI. CONCLUSION

This study proposed a 5G system that applies simplified UTW-OFDM and a receiver-side signal processing technique that mitigates the degradation of receive quality due to the effects of UTW applied at the transmitter side. First, we investigated the LLR adjustment effect in the simplified UTW-OFDM applied 5G system. In addition, an ICI canceller based on the scheme proposed with additional improvements was developed and applied to suppress noise enhancement effects. Computer simulations and experimental studies using SDR evaluated these proposed receiving technologies for the simplified UTW-OFDM-utilized 5G. Computer simulations showed that simplified UTW-OFDM suppressed PSD at the channel edge by up to 54.8 dB compared to CP-OFDM. Furthermore, by using the LLR adjustment technique and the proposed optimal ICI canceller, the problem of BLER degradation at high SNR was solved, and BLER $= 10^{-1}$ was achieved even when applying the maximum value of $N_{TR} = 256$ with MCS $= 18$. Further, experiments with the SDR system confirmed that the OOBE suppression was sufficiently effective, although the OOBE suppression performance was degraded owing to the quantization error. The proposed optimal ICI canceller was also shown to improve the BLER characteristics in SDR experiments and to be applicable to time-domain windows with long transition lengths.

REFERENCES

[1] Y. Ichikawa, K. Mizutani, and H. Harada, "Inter-carrier interference cancellation for 5G system applying simplified universal time-domain windowed OFDM," in *Proc. IEEE 94th Veh. Technol. Conf.*, 2021, pp. 1–5.

[2] The fifth generation mobile communications promotion forum, "5G mobile communications systems for 2020 and beyond," 5GMF White Paper, Version 1.1. Sep. 2017. Accessed: Jun. 13, 2023. [Online]. Available: https://5gmf.jp/wp/wp-content/uploads/2017/10/5GMF-White-Paper-v1_1-All.pdf

[3] MIC, Japan, "Frequency reorganization action plan (revised version for FY 2022)," pp. 1–36. Apr. 2022. Accessed: Jun. 13, 2023. [Online]. Available: https://www.tele.soumu.go.jp/resource/e/freq/process/actionplan.pdf

[4] P. Ahokangas et al., "Business models for local 5G micro operators," *IEEE Trans. Cogn. Commun. Netw.*, vol. 5, no. 3, pp. 730–740, Sep. 2019.

[5] M. Matinmikko, S. Yrjölä, V. Seppänen, P. Ahokangas, H. Hämmäinen, and M. Latva-Aho, "Analysis of spectrum valuation elements for local 5G networks: Case study of 3.5-GHz band," *IEEE Trans. Cogn. Commun. Netw.*, vol. 5, no. 3, pp. 741–753, Sep. 2019.

[6] N. Bhusan et al., "Network densification: The dominant theme for wireless evolution into 5G," *IEEE Signal Process. Mag.*, vol. 52, no. 2, pp. 82–89, Feb. 2014.

[7] E. Memisoglu, A. B. Kihero, E. Basar, and H. Arslan, "Guard band reduction for 5G and beyond multiple numerologies," *IEEE Commun. Lett.*, vol. 24, no. 3, pp. 644–647, Mar. 2020.

[8] A. Goldsmith, *Wireless Communications*. Cambridge, U.K.: Cambridge Univ. Press, 2005.

[9] 3GPP, "LTE; Evolved Universal Terrestrial Radio Access (E-UTRA); Physical channels and modulation," 3GPP Tech. Specification 36.211 V13.2.0, Jun. 2016.

[10] C. Ball, T. Hindelang, I. Kambourov, and S. Eder, "Spectral efficiency assessment and radio performance comparison between LTE and WiMAX," in *Proc. IEEE 19th Int. Symp. Pers., Indoor Mobile Radio Commun.*, 2008, pp. 1–6.

[11] T. Sanguanpuak, D. Niyato, N. Rajatheva, and M. Latva-Aho, "Radio resource sharing and edge caching with latency constraint for local 5G operator: Geometric programming meets stackelberg game," *IEEE Trans. Mobile Comput.*, vol. 20, no. 2, pp. 707–721, Feb. 2021.

[12] X. Huang, J. A. Zhang, and Y. J. Guo, "Out-of-band emission reduction and a unified framework for precoded OFDM," *IEEE Commun. Mag.*, vol. 53, no. 6, pp. 151–159, Jun. 2015.

[13] B. Farhang-Boroujeny, "OFDM versus filter bank multicarrier," *IEEE Signal Process. Mag.*, vol. 28, no. 3, pp. 92–112, May 2011.

[14] Y. Medjahdi, D. le Ruyet, F. Bader, and L. Martinod, "Integrating LTE broadband system in PMR band: OFDM vs. FBMC coexistence capabilities and performances," in *Proc. 11th Int. Symp. Wireless Commun. Syst.*, 2014, pp. 643–648.

[15] V. Vakilian, T. Wild, F. Schaich, S. T. Brink, and J.-F. Frigon, "Universal-filtered multi-carrier technique for wireless systems beyond LTE," in *Proc. IEEE Globecom Workshops*, 2013, pp. 223–228.

[16] J. Abdoli, M. Jia, and J. Ma, "Filtered OFDM: A new waveform for future wireless systems," in *Proc. IEEE 16th Int. Workshop Signal Process. Adv. Wireless Commun.*, 2015, pp. 66–70.

[17] S. Y. Chang, "Spectra and Bandwidth Overhead with and without Filtering for TG4m OFDM," Doc.: IEEE802.15-12-0377-00-004m. Jul. 2012, Accessed: Jun. 13, 2023. [Online]. Available: https://mentor.ieee.org/802.15/documents?is_dcn=377

[18] C. Suschallik, "Improving an OFDM reception using an adaptive Nyquist windowing," *IEEE Trans. Consum. Electron.*, vol. 42, no. 8, pp. 259–269, Aug. 1996.

[19] T. Onizawa, M. Mizoguchi, M. Morikura, and T. Tanaka, "A fast synchronization scheme of OFDM signals for high-rate wireless LAN," *Inst. Electron., Inf. Commun. Engineers Trans. Commun.*, vol. 82, no. 2, pp. 455–463, Feb. 1999.

[20] K. Mizutani, Z. Lan, and H. Harada, "Time-domain windowing design for IEEE 802.11af based TVWS-WLAN systems to suppress out-of-band emission," *Inst. Electron., Inf. Commun. Engineers Trans. Commun.*, vol. 97, no. 4, pp. 875–885, Apr. 2014.

[21] K. Mizutani, T. Matsumura, and H. Harada, "Comprehensive performance evaluation of universal time-domain windowed OFDM-based LTE downlink system," *Inst. Electron., Inf. Commun. Engineers Trans. Commun.*, vol. 102, no. 8, pp. 1728–1740, Aug. 2019.

[22] R. Yokoyama, K. Mizutani, T. Matsumura, and H. Harada, "UTW-OFDM-based 5G new radio with low out-of-band emission," in *Proc. IEEE 22nd Int. Symp. Wireless Pers. Multimedia Commun.*, 2019, pp. 1–6.

[23] A. Yoshito, K. Mizutani, T. Matsumura, and H. Harada, "A frequency-domain ICI cancellation using weight matrix based on window shape for simplified UTW-OFDM," in *Proc. 21st Int. Symp. Wireless Pers. Multimedia Commun.*, 2018, pp. 647–652.
[24] Qualcomm Inc., "Waveform candidates," 3GPP TSG-RAN WG1 #84b, R1-162199. Apr. 2016. Accessed: Jun. 13, 2023. https://www.3gpp.org/ftp/tsg_ran/WG1_RL1/TSGR1_84b/Docs
[25] M. H. N. Shaikh, V. A. Bohara, and A. Srivastava, "Spectral analysis of a nonlinear WOLA-OFDM system with DPD," in *Proc. IEEE Nat. Conf. Commun.*, 2020, pp. 1–4.
[26] K. Ohno and D. Echizenya, "Spectrum notch forming and performance improvement scheme for windowed OFDM," in *Proc. IEEE Int. Conf. Consum. Electron.*, 2021, pp. 1–6.
[27] L. Dan, C. Zhang, J. Yuan, P. Wen, and B. Fu, "Improved N-continuous OFDM using adaptive power allocation," in *Proc. IEEE 8th Annu. Comput. Commun. Workshop Conf.*, 2018, pp. 937–940.
[28] S. Mori, K. Mizutani, and H. Harada, "Software-defined radio-based 5G physical layer experimental platform for highly mobile environments," *IEEE Open J. Veh. Technol.*, vol. 4, pp. 230–240, 2023.
[29] A. Nakamura and M. Itami, "Zero-forcing ICI canceller using iterative detection for mobile reception of OFDM," in *Proc. IEEE Int. Conf. Consum. Electron.*, 2014, pp. 153–154.
[30] S. Suyama, H. Suzuki, and K. Fukawa, "An OFDM receiver employing turbo equalization for multipath environments with delay spread greater than the guard interval," in *Proc. IEEE Semiannual Veh. Technol. Conf.*, 2003, pp. 632–636.
[31] C. W. Huang, P. A. Ting, and C. C. Huang, "A novel message passing based MIMO-OFDM data detector with a progressive parallel ICI canceller," *IEEE Trans. Wireless Commun.*, vol. 10, no. 4, pp. 1260–1268, Apr. 2021.
[32] 3GPP, "5G; NR; Physical channels and modulation," 3GPP Tech. Specification 38.211 V15.7.0, Sep. 2019.
[33] 3GPP, "5G; NR; Multiplexing and channel coding," 3GPP Tech. Specification 38.212 V15.7.0, Sep. 2019.
[34] 3GPP, "5G; NR; Physical layer procedures for control," 3GPP Tech. Specification 38.213 V15.8.0, Dec. 2019.
[35] 3GPP, "Evolved universal terrestrial radio access (E-UTRA); User equipment (UE) radio transmission and reception," 3GPP Tech. Rep. 36.803 V1.1.0, Apr. 2008.
[36] 3GPP, "5G; NR; Physical layer procedures for data," 3GPP Tech. Specification 38.214 V15.2.0, Jun. 2018.

YUU ICHIKAWA received the B.E. degree in electric and electrical engineering in 2021 from the Kyoto University, Kyoto, Japan, where he is currently working toward the M.I. degree with the Graduate School of Informatics, Kyoto University. His current research focuses on wireless mobile communication systems. He was the recipient of the Student Award from IEICE SRW technical committee in 2022, and Student Paper Award from IEEE VTS Tokyo/Japan Chapter in 2022.

KEIICHI MIZUTANI (Member, IEEE) received the B.E. degree in engineering from Osaka Prefecture University, Sakai, Japan, in 2007, and the M.E. and Ph.D. degrees in engineering from the Tokyo Institute of Technology, Tokyo, Japan, in 2009 and 2012, respectively. He is currently an Associate Professor with the Graduate School of Informatics, Kyoto University, Kyoto, Japan. In 2010, he was an invited Researcher with Fraunhofer Heinrich Hertz Institute, Germany. From 2012 to 2014, he was a Researcher with the National Institute of Information and Communications Technology. From 2014 to 2021, he was an Assistant Professor with the Graduate School of Informatics, Kyoto University. From 2021 to 2022, he was an Associate Professor with the School of Platforms, Kyoto University. His current research interests include physical layer technologies in white space communications, dynamic spectrum access, wireless smart utility networks, and 4G/5G/6G systems, including OFDM, OFDMA, MIMO, multi-hop relay network, and full-duplex cellular systems. Since joining in NICT, he has been involved in IEEE 802 standardization activities, namely 802.11af, 802.15.4m, and 802.22b. He was the recipient of the Special Technical Awards from IEICE SR technical committee in 2009 and 2017, Best Paper Award from IEICE SR technical committee in 2010 and 2020, Young Researcher's Award from IEICE SRW technical committee in 2016, Best Paper Award from WPMC2017 and WPMC2020, and Best Paper Presentation Award (1st Place) from IEEE WF-IoT 2020.

HIROSHI HARADA (Member, IEEE) is currently a Professor with the Graduate School of Informatics, Kyoto University, Kyoto, Japan, and the Research Executive Director of the Wireless Networks Research Center, National Institute of Information and Communications Technology (NICT). In 1995, he joined the Communications Research Laboratory, Ministry of Posts and Communications (currently, NICT). From 2005 to 2014, he was a Visiting Professor with the University of Electro-Communications, Tokyo, Japan. In 2014, he was a Professor with Kyoto University. He has authored the book titled *Simulation and Software Radio for Mobile Communications* (Artech House, 2002). Since 1995, his research interests include software defined radio, cognitive radio, dynamic spectrum access network, wireless smart ubiquitous network, and broadband wireless access systems on VHF, UHF, microwave, and millimeter-wave bands. He has also joined many standardization committees and forums in the United States and in Japan and fulfilled important roles for them, especially IEEE 1900 and IEEE 802. He was the Chair of IEEE DySpan Standards Committee and a vice chair of IEEE 802.15.4g, IEEE 802.15.4m, 1900.4, and TIA TR-51. He was the Board of Directors of IEEE communication society standards board, SDR forum, DSA alliance, and WhiteSpace alliance. From 2012 to 2019, he was a Cofounder of Wi-SUN alliance and was the Chairman of the board. He is currently the Vice Chair of IEEE 2857, IEEE 802.15.4aa and Wi-SUN alliance. He was also the Chair of the IEICE Technical Committee on Software Radio and Public Broadband Mobile Communication Development Committee, ARIB. He is also involved in many other activities related to telecommunications. He was the recipient of the achievement awards in 2006 and 2018 and Fellow of IEICE in 2009, respectively and the achievement awards of ARIB in 2009, 2018, and 2022, respectively, on the topic of research and development on cognitive radio and wireless smart utility network.